The Closely Related RNA helicases, UAP56 and URH49, Preferentially Form Distinct mRNA Export Machineries and Coordinately Regulate Mitotic Progression

Tomohiro Yamazaki,* Naoko Fujiwara,* Hiroko Yukinaga,* Miki Ebisuya,*† Takuya Shiki,* Tomoya Kurihara,* Noriyuki Kioka,‡ Taiho Kambe,* Masaya Nagao,* Eisuke Nishida,* and Seiji Masuda*

*Division of Integrated Life Science, Graduate School of Biostudies, and ‡Division of Applied Life Sciences, Graduate School of Agriculture, Kyoto University, Kyoto 606-8502, Japan; and †Career-Path Promotion Unit for Young Life Scientists, Kyoto University, Kyoto 606-8501, Japan

Nuclear export of mRNA is an essential process for eukaryotic gene expression. The TREX complex couples gene expression from transcription and splicing to mRNA export. Sub2, a core component of the TREX complex in yeast, has diversified in humans to two closely related RNA helicases, UAP56 and URH49. Here, we show that URH49 forms a novel URH49–CIP29 complex, termed the AREX (alternative mRNA export) complex, whereas UAP56 forms the human TREX complex. The mRNAs regulated by these helicases are different at the genome-wide level. The two sets of target mRNAs contain distinct subsets of key mitotic regulators. Consistent with their target mRNAs, depletion of UAP56 causes mitotic delay and sister chromatid cohesion defects, whereas depletion of URH49 causes chromosome arm resolution defects and failure of cytokinesis. In addition, depletion of the other human TREX components or CIP29 causes mitotic defects similar to those observed in UAP56- or URH49-depleted cells, respectively. Taken together, the two closely related RNA helicases have evolved to form distinct mRNA export machineries, which regulate mitosis at different steps.

INTRODUCTION

In eukaryotic cells, protein-coding genes are transcribed as a pre-mRNA in the nucleus and the pre-mRNA undergoes several RNA processing steps, such as 5′-capping, splicing and 3′-end processing. The mature mRNA is exported from the nucleus to the cytoplasm. These gene expression processes are tightly coordinated with each other, to achieve efficient and accurate gene expression (Maniatis and Reed, 2002; Orphanides and Reinberg, 2002; Komili and Silver, 2008).

After the mRNA processing steps, the mRNA–protein complex is mature and ready for nuclear export. Initial studies of the mRNA export pathway were conducted in *Saccharomyces cerevisiae*, leading to the identification of the key components of the mRNA export machinery (Reed and Hurt, 2002; Vinciguerra and Stutz, 2004; Aguilera, 2005; Kohler and Hurt, 2007). Among them, the TREX complex is evolutionarily conserved and plays a critical role in coupling

transcription and splicing to mRNA export (Jimeno *et al.,* 2002; Strasser *et al.,* 2002; Masuda *et al.,* 2005; Reed and Cheng, 2005; Cheng *et al.,* 2006; Katahira *et al.,* 2009). The human TREX (hTREX) complex is composed of the multimeric human THO (hTHO) complex, containing hTho2/THOC2, hHpr1/THOC1, fSAP79/THOC5, fSAP35/THOC6, fSAP24/THOC7 and hTex1/THOC3, the DECD-box RNA helicase UAP56 (Sub2 in *S. cerevisiae*), and the mRNA export adaptor protein Aly/THOC4 (Yra1 in *S. cerevisiae*; Masuda *et al.,* 2005). The hTREX complex is recruited to the 5′ cap site of the mRNA via an interaction between Aly and the cap-binding complex (CBC; CBP80 and CBP20) during splicing (Cheng *et al.,* 2006; Nojima *et al.,* 2007), ensuring mRNA export to the cytoplasm in a 5′-to-3′ direction. Aly is in turn recognized by Tap/NXF1 (Mex67 in *S. cerevisiae*), which is an essential mRNA export receptor. Then the mRNA–protein complex passes through the nuclear pore complex (Luo *et al.,* 2001; Rodrigues *et al.,* 2001; Strasser and Hurt, 2001; Katahira *et al.,* 2009). In addition to Aly, SR proteins, which are regulators of pre-mRNA splicing, also function as adaptor proteins to recruit Tap onto mRNA (Huang *et al.,* 2003). Tap is believed to stand at the final step of the mRNA export pathway for most mRNAs and to integrate several mRNA export pathways (Katahira *et al.,* 1999; Cullen, 2003; Stutz and Izaurralde, 2003).

These key mRNA export factors have a conserved role in other organisms although there are some functional differences. Recently, genome-wide RNA interference (RNAi) screening identified the factors required for mRNA export in *Drosophila melanogaster* (Farny *et al.,* 2008). Some of the identified factors were conserved with yeast, and some were not. In addition, several key mRNA export factors have diversi-

Abbreviations used: AREX, alternative mRNA export; CBC, cap-binding complex; CPC, chromosomal passenger complex; DAPI, 4′,6-diamidino-2-phenylindole; FISH, fluorescent in situ hybridization; GO, gene ontology; MCD, mitotic cell death; NE, nuclear extract; NEBD, nuclear envelope breakdown; PMSCS, premature sister chromatid separation; SAC, spindle assembly checkpoint.
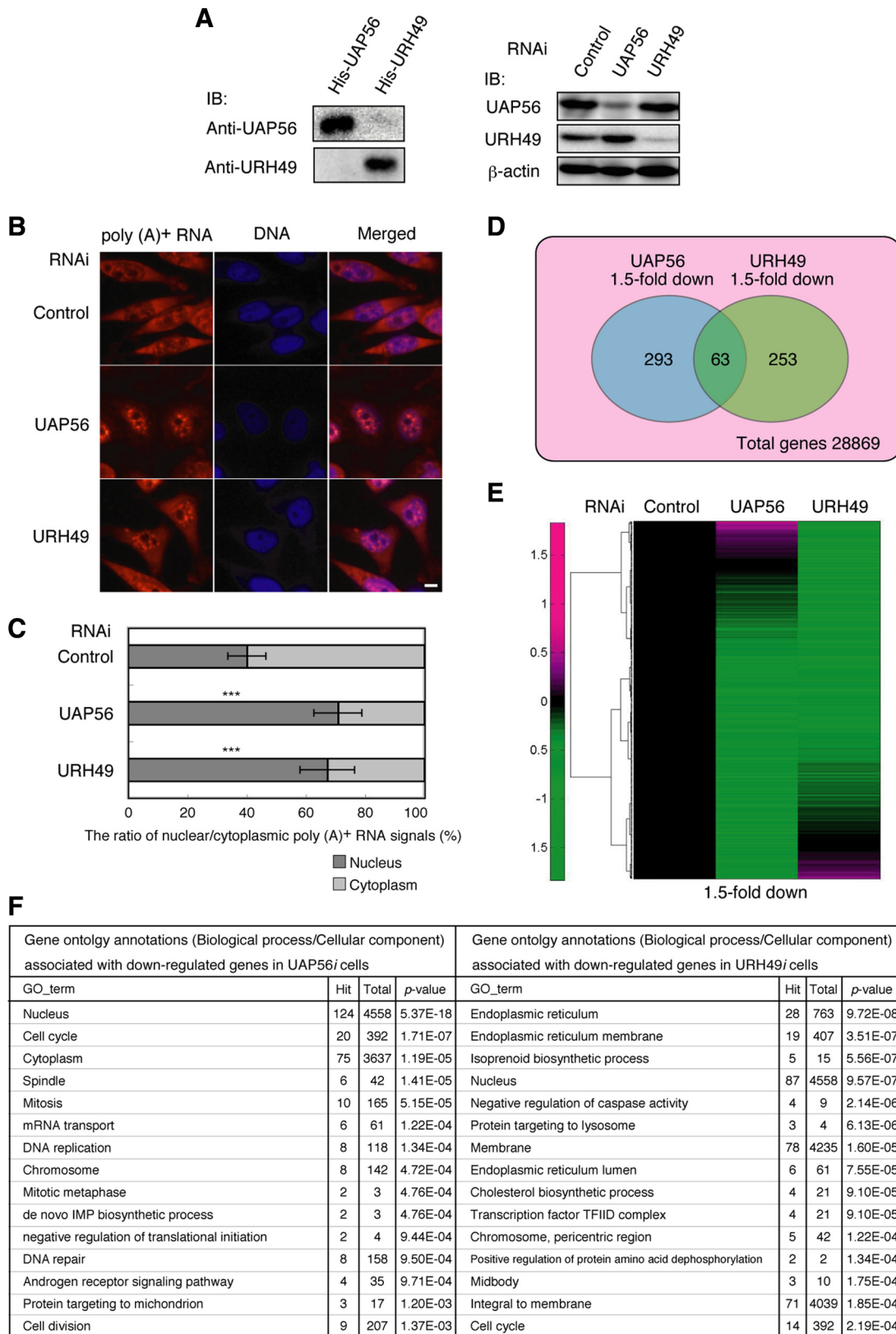
A Left IB: Anti-UAP56, Anti-URH49; His-UAP56, His-URH49. Right RNAi: Control, UAP56, URH49; IB: UAP56, URH49, β-actin.

B poly (A)+ RNA, DNA, Merged; RNAi Control, UAP56, URH49.

C The ratio of nuclear/cytoplasmic poly (A)+ RNA signals (%); RNAi Control, UAP56, URH49. Nucleus, Cytoplasm.

D UAP56 1.5-fold down, URH49 1.5-fold down. 293, 63, 253. Total genes 28869.

E RNAi Control, UAP56, URH49. 1.5-fold down.

F

Gene ontolgy annotations (Biological process/Cellular component) associated with down-regulated genes in UAP56*i* cells				Gene ontolgy annotations (Biological process/Cellular component) associated with down-regulated genes in URH49*i* cells			
GO_term	Hit	Total	*p*-value	GO_term	Hit	Total	*p*-value
Nucleus	124	4558	5.37E-18	Endoplasmic reticulum	28	763	9.72E-08
Cell cycle	20	392	1.71E-07	Endoplasmic reticulum membrane	19	407	3.51E-07
Cytoplasm	75	3637	1.19E-05	Isoprenoid biosynthetic process	5	15	5.56E-07
Spindle	6	42	1.41E-05	Nucleus	87	4558	9.57E-07
Mitosis	10	165	5.15E-05	Negative regulation of caspase activity	4	9	2.14E-06
mRNA transport	6	61	1.22E-04	Protein targeting to lysosome	3	4	6.13E-06
DNA replication	8	118	1.34E-04	Membrane	78	4235	1.60E-05
Chromosome	8	142	4.72E-04	Endoplasmic reticulum lumen	6	61	7.55E-05
Mitotic metaphase	2	3	4.76E-04	Cholesterol biosynthetic process	4	21	9.10E-05
de novo IMP biosynthetic process	2	3	4.76E-04	Transcription factor TFIID complex	4	21	9.10E-05
negative regulation of translational initiation	2	4	9.44E-04	Chromosome, pericentric region	5	42	1.22E-04
DNA repair	8	158	9.50E-04	Positive regulation of protein amino acid dephosphorylation	2	2	1.34E-04
Androgen receptor signaling pathway	4	35	9.71E-04	Midbody	3	10	1.75E-04
Protein targeting to michondrion	3	17	1.20E-03	Integral to membrane	71	4039	1.85E-04
Cell division	9	207	1.37E-03	Cell cycle	14	392	2.19E-04

Figure 1. UAP56*i* and URH49*i* affect the expression of different subsets of genes at the genome-wide level. (A) Left, UAP56 and URH49 antibodies specifically recognized recombinant His-UAP56 and His-URH49 purified from *Escherichia coli*, respectively. IB, immunoblotting. Right, specific knockdown of UAP56 or URH49 was confirmed by immunoblotting. HeLa cells transfected with the indicated siRNAs were cultured for 48 h. β-actin was used as a loading control. IB, immunoblotting. (B) The localization of poly(A)+ RNA in HeLa cells transfected with the indicated siRNAs was analyzed by RNA-FISH after 48 h. Scale bar, 10 μm. (C) The ratio of nuclear and cytoplasmic poly(A)+ RNA signals was quantified in each knockdown cell. Each value is the mean with SD. p values were calculated by comparison with the control:

fied throughout evolution and form protein families in higher eukaryotes (Stutz and Izaurralde, 2003; Wolyniak and Cole, 2008). Therefore, investigation into the diversity among mRNA export pathways is warranted.

In the TREX complex, UAP56 homologues (Sub2 in *S. cerevisiae*, UAP56 in *C. elegans*, and Hel25E in *D. melanogaster*) are essential in each species, indicating that this RNA helicase plays a critical role in mRNA export (Strasser and Hurt, 2001; Herold *et al.*, 2003; MacMorris *et al.*, 2003). In mammals, there is a Sub2 homolog other than UAP56, URH49/DDX39 (Pryor *et al.*, 2004). UAP56 and URH49 show extensive homology; their amino acid identity is 90% and similarity is 96%. Both UAP56 and URH49 can rescue the lethality of a yeast strain lacking the Sub2 gene, suggesting that UAP56 and URH49 exert similar functions in *S. cerevisiae*. It has been reported that UAP56 associates with the hTHO complex and Aly to form the hTREX complex (Masuda *et al.*, 2005). Yeast two-hybrid screening identified the interaction between UAP56 and CIP29 as well as that between URH49 and CIP29 (Leaw *et al.*, 2004). UAP56 and URH49 directly interact with Aly as well as CIP29 in vitro (Leaw *et al.*, 2004; Pryor *et al.*, 2004; Sugiura *et al.*, 2007b). However, it remains unclear what kind of complex is formed by UAP56 or URH49 under physiological conditions in human cells and whether the two closely related RNA helicases have separate functions.

In this study, we examined the function of UAP56 and URH49 in human cells, to investigate diversity in the mRNA export pathways and the biological importance of these helicases. Here, we provide the first evidence that UAP56 and URH49 preferentially form the hTREX complex and the newly identified URH49–CIP29 mRNA export complex, which is termed the AREX (alternative mRNA export) complex, respectively. Each helicase regulates a specific subset of genes involved in mitosis. Consistent with their target genes, knockdown of either UAP56 or URH49 resulted in different mitotic defects. These findings provide new insight into the gene expression networks regulated by the mRNA processing/export machinery.

MATERIALS AND METHODS

Antibodies

Rat polyclonal antibodies to Aly and CIP29 were raised against full-length proteins fused to glutathione-*S*-transferase (GST). The rat polyclonal antibody specific to UAP56 was raised against amino acids 1–35 of UAP56 fused to GST. The URH49-specific rat polyclonal antibody was obtained in two steps. First, antiserum recognizing amino acids 1–34 of URH49 was obtained. Second, antibodies reacting to UAP56 were removed from the URH49 antiserum. Anti-Aly, hTho2, hHpr1, fSAP79, and fSAP24 rabbit polyclonal antibodies have been described previously (Masuda *et al.*, 2005). Commercial antibodies used were as follows: anti-β-tubulin mouse monoclonal antibodies (Sigma, St. Louis, MO) and anti-β-actin (Sigma), anti-BRCA1 (C-20; Santa Cruz, CA),

anti-claspin (Sigma), anti-survivin (Abnova, Taipei City, Taiwan), and anti-PRC1 (BioLegend, San Diego, CA) rabbit polyclonal antibodies.

Cell Culture and Transfection

All cell lines used in this study were maintained in DMEM (Sigma) supplemented with 10% heat-inactivated fetal bovine serum at 37°C. Transient transfection of plasmid (0.8 μg/ml) or small interfering RNA (siRNA; 20 nM) was performed using Lipofectamine 2000 reagent (2 μl/ml; Invitrogen, Carlsbad, CA) according to the manufacturer's instructions.

Plasmids and siRNAs

To construct the below plasmids, the fragments were obtained by PCR amplification with the addition of restriction enzyme sites at both ends. Enhanced green fluorescent protein (EGFP)-UAP56 and DsRed-URH49 were generated by the insertion of the UAP56 or URH49 open reading frame into the HindIII and KpnI sites of pEGFP-C1 and pDsRed-monomer-C1, respectively. The correct construction of the plasmids was confirmed by sequencing. The siRNAs used in this study are listed in Supplemental Table S1.

Immunoprecipitation and Immunoblotting

Nuclear extract (NE) and mini-scale preparations of NE were produced as described previously (Andrews and Faller, 1991; Abmayr and Workman, 1993). Immunoprecipitations was performed as described (Masuda *et al.*, 2005). For immunoblotting, anti-mouse or anti-rabbit TrueBlot ULTRA antibodies conjugated with horseradish peroxidase (HRP; eBioscience, San Diego, CA) or HRP-conjugated anti-rat light chain–specific antibody (Jackson ImmunoResearch, West Grove, PA) were used as secondary antibodies to detect immunoprecipitated samples.

Immunofluorescence

Cells (5–10% confluency) cultured on glass coverslips were transfected with siRNA or plasmid. After transfection, cells were cultured for 48 h, fixed in 4% formaldehyde in phosphate-buffered saline (PBS) and permeabilized with 0.1% Triton X-100 in PBS. After blocking with 6% bovine serum albumin (BSA) in PBS, the coverslips were incubated with primary antibodies in 2% BSA in PBS followed by secondary antibodies conjugated with Alexa-488 or Alexa-594 (Molecular Probes, Eugene, OR). DNA was stained with DAPI.

RNA Fluorescence In Situ Hybridization

Cells (5–10% confluency) on coverslips were cultured for 48 h after siRNA transfection, fixed in 10% formaldehyde in PBS for 20 min, and permeabilized in 0.1% Triton X-100 in PBS for 10 min. Cells were washed three times with PBS for 10 min and once with 2× SSC for 5 min, prehybridized with ULTRAhyb-Oligo Hybridization Buffer (Ambion, Austin, TX) for 1 h at 42°C in a humidified chamber, and then incubated overnight with 20 pmol Cy3-labeled oligo-(d)T$_{45}$ probe diluted in hybridization buffer. Cells were washed for 20 min at 42°C with 2× SSC, 0.5× SSC, and then 0.1× SSC. Quantification of the proportions of nuclear and cytoplasmic poly(A)$^+$ RNA signals in 50 cells was performed using ImageGauge (Fuji, Tokyo, Japan; Valencia *et al.*, 2008).

Live Cell Imaging

Cells (5–10% confluency) grown on 35-mm glass-bottom dishes (Iwaki, Holliston, MA) were transfected with siRNA. After transfection, cells were cultured for 36 h and then imaged every 1 or 5 min at 37°C in 5% CO$_2$ with 100% humidity for 16 h, using an IX-81 microscope equipped with a time-lapse imaging system (Olympus, Melville, NY), FV10i (Olympus), and BZ9000 (Keyence, Osaka, Japan).

Mitotic Chromosome Spreads

Cells (5–10% confluency) were grown in 12-well plates and cultured for 48 h after transfection with siRNA. After treatment with 100 ng/ml colcemid (Sigma) for 6 h, all cells were collected, washed twice with PBS, and then swollen with hypotonic buffer (0.03 M sodium citrate) at 37°C for 25 min. Cells were washed once with Calnoy's solution (three parts methanol to one part acetic acid), fixed with the same solution, dropped onto glass slides using a pointed Pasteur pipette, and then dried and stained with DAPI.

Genome-Wide Gene Expression Analysis by Oligonucleotide Microarray

HeLa cells (5–10% confluency) were transfected with *UAP56*- or *URH49*-siRNA and cultured for 48 h. Then, cytoplasmic RNA was isolated as described (Gilman, 1997), and the quality was confirmed by RT-PCR as shown in Supplemental Figure S1A. Three independent array experiments were conducted. Array experimental procedures were performed according to manufacturer's instructions. Human Gene 1.0 ST arrays (Affymetrix, Santa Clara, CA) were used. The probe set signals were calculated using the Affymetrix Expression Console (PM background correction, quantile normalization, iterPLIER). Gene ontology (GO) annotation referred to an annotation file (version Na26_hg18) from Affymetrix. For each GO term, the distribution

Figure 1 (cont). ***p < 0.001, Student's *t* test. (D) The Venn diagram represents transcripts reduced at least 1.5-fold in UAP56*i* or URH49*i* cells. There are 28,869 probe sets on the array chip. The number in each circle indicates the number of genes detected. (E) Gene expression profiles in UAP56*i* or URH49*i* cells were compared with control cells by hierarchical clustering analysis. The threshold was set at a 1.5-fold reduction. (F) Genes down-regulated at least 1.5-fold in UAP56*i* or URH49*i* cells were enriched for several gene ontology (GO) terms categorized in "Biological Process" and "Cellular Component". Fifteen GO terms are listed in order of their p values. Hit indicates the number of down-regulated genes in UAP56*i* or URH49*i* cells. Total indicates the number of genes categorized in each GO term.
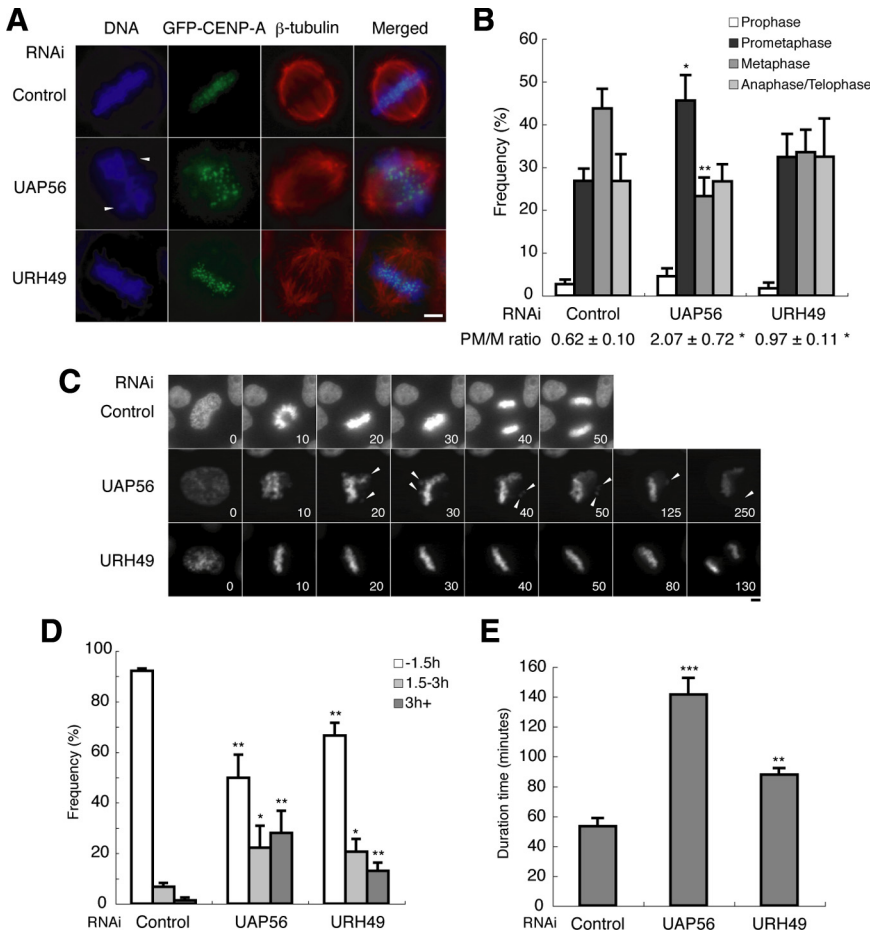
Figure 2. UAP56*i* and URH49*i* result in mitotic progression defects. (A) Typical mitotic figures are shown in the indicated siRNA-transfected HeLa cells expressing GFP-CENP-A. GFP-CENP-A and β-tubulin signals indicate the location of the centromere and spindle body, respectively. The arrowhead indicates the misaligned chromosome. Scale bar, 10 μm. (B) The proportion of each mitotic phase is shown in each knockdown cell. Each value is the mean with SD of three independent experiments (more than 70 mitotic cells were evaluated in each experiment). The ratios of cells in prometaphase to metaphase (PM/M ratio) are shown as the means with SD of three independent experiments. p values were calculated by comparison with the control: *p < 0.05, **p < 0.01, Student's *t* test. (C) Representative successive live cell images for the indicated siRNA-transfected HeLa cells expressing H2B-GFP. The number at the bottom right indicates the time (min) from nuclear envelope breakdown (NEBD). The arrowhead indicates the misaligned chromosome. Scale bar, 10 μm. (D) The time from NEBD to anaphase transition or mitotic cell death (MCD; Duration time) was measured and classified into three groups as follows: −1.5 h, duration was within 1.5 h; 1.5–3 h, from 1.5 h to 3 h; 3 h+, more than 3 h. Cells were observed 36–52 h after siRNA transfection, and the time was measured by analyzing the recordings. The means and SDs of three independent experiments were calculated. At least 30 cells were observed in each experiment. p values were calculated by comparison with the control: *p < 0.05, **p < 0.01, Student's *t* test. (E) The duration is shown as the means with SD of three independent experiments. p values were calculated by comparison with the control: **p < 0.01, ***p < 0.001, Student's *t* test.

of at least 1.5-fold down-regulated genes in *UAP56*-knockdown and *URH49*-knockdown cells was compared with that in the total probe set (Fisher test). The microarray data were submitted to Gene expression omnibus (GEO; accession number: GSE18173).

Real-Time PCR

cDNA was synthesized from cytoplasmic RNA (1 μg) by reverse transcription using 10 U SuperScript III (Invitrogen) and random primers. Real-time PCR was performed with Thunderbird SYBR qPCR Mix (TOYOBO, Osaka, Japan) and analyzed on an ABI Prism 7700 (Applied Biosystems, Carlsbad, CA). Primer sets for this analysis are described in Supplemental Table S2, Carlsbad, CA.

RESULTS

### Different Genome-Wide Gene Expression Profiles in UAP56 and URH49 Knockdown Cells

To reveal the in vivo biological functions of UAP56 and URH49, either UAP56 or URH49 was specifically knocked down in HeLa cells. Specific antibodies against UAP56 and URH49 were raised (Figure 1A). Each siRNA efficiently knocked down its corresponding mRNA, and therefore protein (Figure 1A). Hereafter, we have added the suffix *i* to indicate knockdown.

UAP56 has a conserved role in the export of bulk poly(A)$^+$ RNA to the cytoplasm. Thus, the effect on the nuclear export of bulk poly(A)$^+$ RNA was examined in UAP56*i* and URH49*i* cells. Either knockdown led to the accumulation of bulk poly(A)$^+$ RNA in the nucleus (Figure 1, B and C; Kapadia *et al.*, 2006; Hautbergue *et al.*, 2009). To identify the mRNAs that were regulated by UAP56 or URH49 at the mRNA processing and export steps, we analyzed the genome-wide gene expression profiles using cytoplasmic RNA (Supplemental Figure S1), on a high-density oligonucleotide microarray containing 28,869 probe sets, which included all human protein coding genes. To compare the gene expression profiles and to focus on genes particularly susceptible to knockdown of UAP56 or URH49, the distribution of transcript expression levels was normalized. The microarray data were validated by semiquantitative RT-PCR and real-time PCR with selected genes (data not shown). Efficient knockdown of *UAP56* mRNA or *URH49* mRNA (~70% reduction) was also confirmed by microarray analyses. A threshold was set at 1.5-fold reduction. Microarray data indicated that 356 or 316 genes were down-regulated in UAP56*i* or URH49*i* cells, respectively (Figure 1D). Among them, 63 genes were decreased in both UAP56*i* and URH49*i* cells. Hierarchical clustering analysis showed that their expression profiles were divided into several major groups with different expression patterns (Figure 1E). These data suggest that particular populations of mRNAs are highly susceptible to either UAP56*i* or URH49*i*, and a substantial fraction of down-regulated genes was different between UAP56*i* and URH49*i* cells.

To investigate whether down-regulated genes in UAP56*i* or URH49*i* cells were functionally associated with particular cellular processes, we classified the down-regulated genes

Figure 3. UAP56*i* leads to premature sister chromatid separation (PMSCS), whereas URH49*i* leads to chromosome arm resolution defects. (A) The phenotypes observed on the mitotic chromosome spreads were categorized into four patterns I to IV as follows: I: sister chromatids were attached at the centromere region, Normal; II: some of the sister chromatids were separated, Partial separation; III: most or all of the sister chromatids were separated, Severe or complete separation; and IV: all sister chromatids were separated and hypercondensed, Complete separation and hypercondensation. The bottom left inset shows high magnification of the mitotic chromosome spread indicated by the dashed square. Scale bar, 10 μm. (B) Representative mitotic chromosome spreads in Control-, UAP56-, and URH49-siRNA transfected cells. The Roman numeral in the top left represents the category as defined in A. The bottom left and right insets represent medium- and high-magnification images of the mitotic chromosome spread(s) indicated by the large and small dashed squares, respectively. Scale bar, 10 μm. (C) The frequency of PMSCS was classified into categories I to IV by analyzing more than 100 cells in each experiment. Each value is the mean with SD of three independent experiments. p values were calculated by comparison with the control: *$p < 0.05$, **$p < 0.01$, ***$p < 0.001$, Student's *t* test. (D) Mitotic chromosome spreads with open and closed arms. The bottom panel is a magnified image of the area indicated by the dashed square. Scale

bar, 10 μm. (E) The frequency of mitotic chromosomes with open and closed arms was obtained by analyzing more than 100 cells in each experiment. Each value is the mean with SD of three independent experiments. p values were calculated by comparison with the control: ***$p < 0.001$, Student's *t* test.
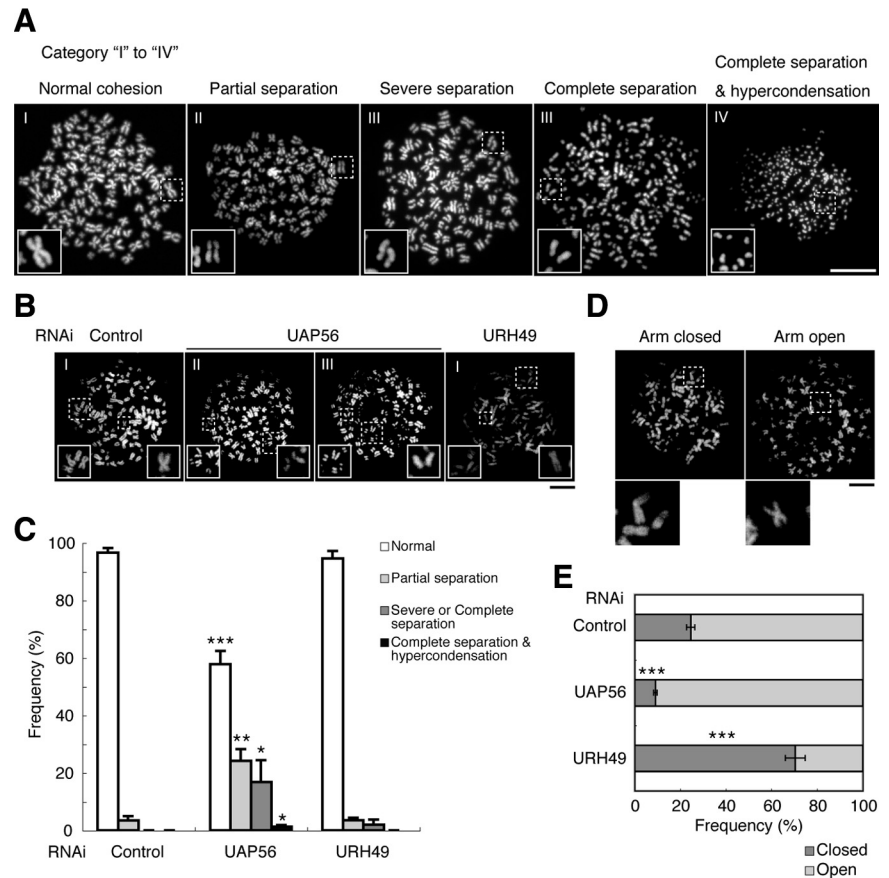
into GO groups by calculating the p value (Supplemental Table S3). In particular, we focused on the GO categories "Biological Process" and "Cellular Component" (Figure 1F). This revealed that several functional classes of genes were significantly enriched in UAP56*i* or URH49*i* cells.

UAP56i and URH49i Result in Mitotic Progression Defects

The lists of genes in these GO categories contained several key mitotic factors (Supplemental Table S3). These data suggest that the absence of either helicase would affect mitotic processes. To explore the functional link between these helicases and mitosis, we investigated mitotic progression using a HeLa cell line stably expressing GFP-CENP-A, which indicates the position of the centromere. Chromosome misalignment in mitotic cells was frequently observed when UAP56 was knocked down (Figure 2A). Chromosome misalignment occurred to some extent when URH49 was knocked down. Chromosome misalignment causes the activation of spindle assembly checkpoint (SAC), which leads to the arrest of mitotic progression at prometaphase (Musacchio and Salmon, 2007; Holland and Cleveland, 2009). To evaluate the mitotic delay, the proportion of cells in each mitotic phase was quantified (Figure 2B). The ratio of prometaphase to metaphase (PM/M ratio) was significantly increased in UAP56*i* and URH49*i* cells, suggesting mitotic delay during prometaphase in UAP56*i* and URH49*i* cells.

We next investigated mitotic progression in detail using live cell imaging of a HeLa cell line stably expressing H2B-

GFP. In control-siRNA transfected cells, cells entered mitosis and chromosomes were aligned at the metaphase plate. Then, the chromosomes were divided into two daughter cells (Figure 2C and Supplemental Movie S1). However, UAP56*i* cells frequently demonstrated chromosome misalignment and mitotic delay at prometaphase (Supplemental Movie S2). These results clearly show that the SAC, activated by chromosome misalignment, arrests mitotic progression in UAP56*i* cells. We measured the time from nuclear envelope breakdown (NEBD) to anaphase transition or mitotic cell death (MCD; DeLuca *et al.*, 2002; Yang *et al.*, 2005), which was sometimes observed in UAP56*i* and URH49*i* cells (data not shown). This time was approximately three times longer in UAP56*i* cells than in control siRNA-transfected cells (Figure 2, D and E). URH49*i* caused a milder mitotic delay than UAP56*i* (Supplemental Movie S3). It was noteworthy that URH49*i* cells demonstrated a low frequency of failure of cytokinesis (Supplementary Figure S2). These observations provide evidence that UAP56 plays an important role in mitotic progression and that URH49 is involved in mitotic progression and cytokinesis to some extent.

UAP56i Leads to Premature Sister Chromatid Separation, Whereas URH49i Leads to Chromosome Arm Resolution Defects

To examine the cause of the mitotic progression defects, mitotic chromosome spreads were prepared from the knockdown cells. In control siRNA-transfected cells, sister chro-
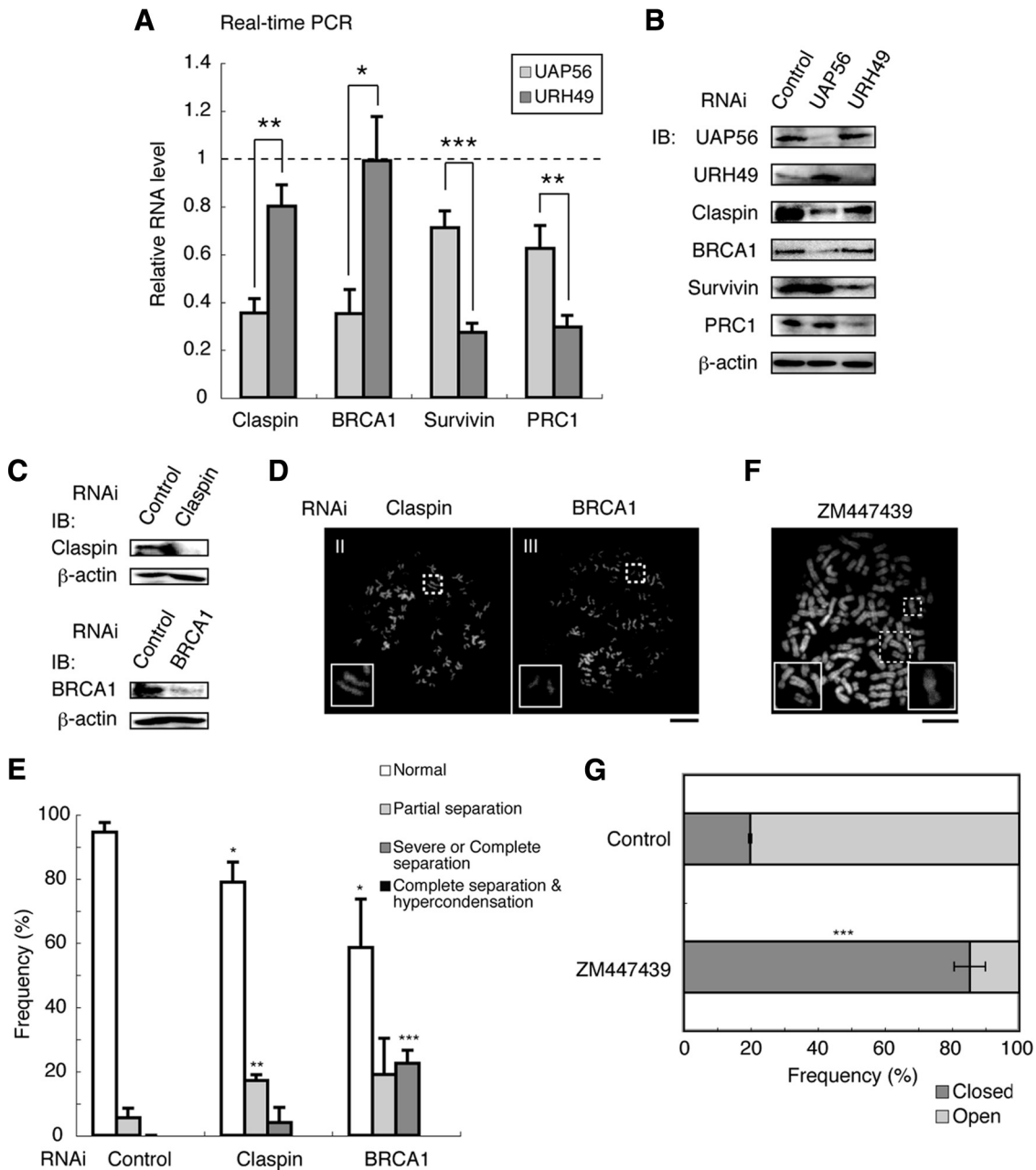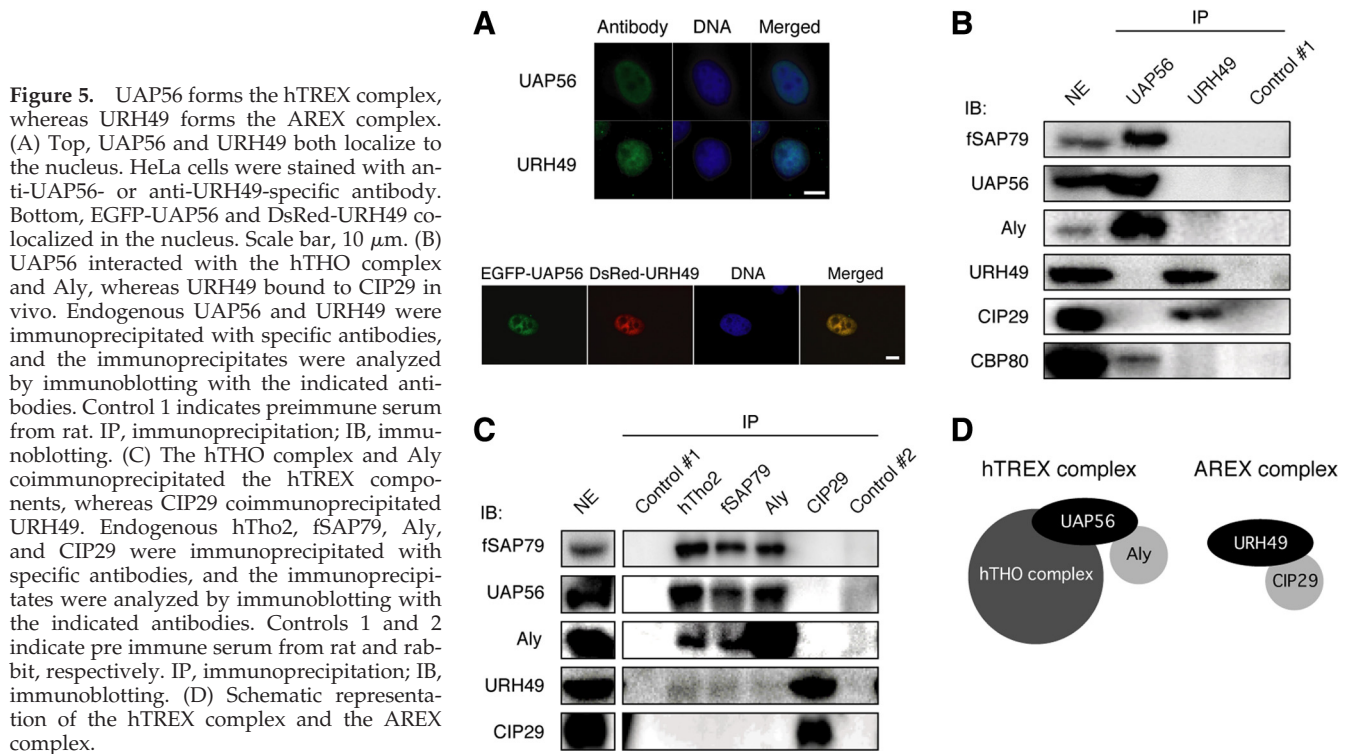
Figure 4. UAP56*i* and URH49*i* lead to down-regulation of genes necessary for mitosis. (A) The expression of *claspin* and *BRCA1* mRNAs was down-regulated in UAP56*i* cells. On the other hand, the expression of *survivin* and *PRC1* was decreased in URH49*i* cells. The relative expression levels were analyzed with real-time RT-PCR and were normalized against the *PGK1* gene. The results shown were derived from three different experiments, with SDs. p values: *p < 0.05, **p < 0.01, ***p < 0.001, Student's *t* test. (B) Immunoblotting for the proteins corresponding to the genes that were reduced in UAP56*i* or URH49*i* cells. β-actin was used as a loading control. IB, immunoblotting. (C) Knockdown of claspin or BRCA1 was confirmed by immunoblotting. HeLa cells transfected with the indicated siRNAs were cultured for 48 h. β-actin was used as a loading control. IB, immunoblotting. (D) Representative mitotic chromosome spreads in *claspin*- and *BRCA1*-siRNA transfected cells. The Roman numeral in the top left represents the category as defined in Figure 3A. The bottom left insets represent high-magnification images of the mitotic chromosome spread(s) indicated by the dashed squares. Scale bar, 10 μm. (E) The frequency of PMSCS was classified into categories I to IV by analyzing more than 100 cells in each experiment. Each value is the mean with SD of three independent experiments. p values were calculated by comparison with the control: *p < 0.05, **p < 0.01, ***p < 0.001, Student's *t* test. (F) Treatment with ZM447439 (BIOMOL; 100 μM for 6 h), an aurora kinase B inhibitor, led to chromosome arm resolution defects. The bottom left and right insets represent medium- and high-magnification images of the mitotic chromosome spread(s) indicated by the large and small dashed squares, respectively. Scale bar, 10 μm. (G) The frequency of mitotic chromosomes with open and closed arms was obtained by analyzing more than 100 cells in each experiment. Each value is the mean with SD of three independent experiments. p values: ***p < 0.001, Student's *t* test.

matids were attached at the centromere (Figure 3, A and B). UAP56*i* often caused premature sister chromatid separation (PMSCS; Figure 3B). In addition, PMSCS occurred after treatment with siRNAs targeting different sites on *UAP56* (Supplemental Figure S3). These results indicate that the PMSCS in UAP56*i* cells was not an off-target effect, but

Figure 5. UAP56 forms the hTREX complex, whereas URH49 forms the AREX complex. (A) Top, UAP56 and URH49 both localize to the nucleus. HeLa cells were stained with anti-UAP56- or anti-URH49-specific antibody. Bottom, EGFP-UAP56 and DsRed-URH49 co-localized in the nucleus. Scale bar, 10 μm. (B) UAP56 interacted with the hTHO complex and Aly, whereas URH49 bound to CIP29 in vivo. Endogenous UAP56 and URH49 were immunoprecipitated with specific antibodies, and the immunoprecipitates were analyzed by immunoblotting with the indicated antibodies. Control 1 indicates preimmune serum from rat. IP, immunoprecipitation; IB, immunoblotting. (C) The hTHO complex and Aly coimmunoprecipitated the hTREX components, whereas CIP29 coimmunoprecipitated URH49. Endogenous hTho2, fSAP79, Aly, and CIP29 were immunoprecipitated with specific antibodies, and the immunoprecipitates were analyzed by immunoblotting with the indicated antibodies. Controls 1 and 2 indicate pre immune serum from rat and rabbit, respectively. IP, immunoprecipitation; IB, immunoblotting. (D) Schematic representation of the hTREX complex and the AREX complex.

resulted from the loss of UAP56 function. To evaluate the extent of chromosome separation, the phenotype of PMSCS was classified into four categories: I to IV (details in the legend to Figure 3A; Tang *et al.*, 2006). UAP56*i* cells often showed category II or III, and some mitotic spreads even exhibited category IV (Figure 3, B and C). In contrast, URH49*i* cells rarely exhibited PMSCS. These results suggest that PMSCS is the cause of chromosome misalignment in UAP56*i* cells.

In contrast, in URH49*i* cells, sister chromatids were often attached at the chromosome arms (Figure 3, B and D). During prophase and prometaphase, sister chromatids become separated in their arm regions (Onn *et al.*, 2008; Peters *et al.*, 2008). Therefore, the frequency of mitotic chromosomes with open and closed arms was evaluated (Figure 3, D and E). The proportion of mitotic chromosomes with closed arms was ~25 and 70% in control and URH49*i* cells, respectively (Figure 3E and Supplementary Figure S3, C and E). UAP56*i* cells displayed more frequent separation in the arms than did the control cells. These results clearly indicate that the mitotic defect in URH49*i* cells is different from that in UAP56*i* cells.

UAP56i and URH49i Affect the Expression of Distinct mRNAs Necessary for Normal Mitosis

UAP56*i* caused PMSCS and mitotic progression defects. Mitotic progression was arrested during prometaphase in UAP56*i* cells, suggesting that the SAC was functional. Therefore, it was unlikely that the PMSCS was caused by early activation of the anaphase-promoting complex/cyclosome. Instead, the likely cause of the PMSCS was the defect in sister chromatid cohesion. Consistent with this phenotype, microarray data, real-time PCR analysis, and immunoblotting showed that UAP56*i* caused the down-regulation of mRNA and protein of both claspin and BRCA1 (Supplemental Table S3 and Figure 4, A and B). It has been reported that

knockdown of BRCA1 results in PMSCS (Chabalier *et al.*, 2006; Skibbens, 2008). In addition, deletion of Mrc1, the yeast homolog of claspin, caused sister chromatid cohesion defects (Warren *et al.*, 2004; Xu *et al.*, 2004). In fact, either claspin*i* or BRCA1*i* led to PMSCS (Figure 4, C–E).

In contrast, URH49*i* resulted in chromosome arm resolution defects and failure of cytokinesis. The microarray data indicated strong down-regulation of *survivin/BIRC5* and *PRC1* mRNA in URH49*i* cells (Supplemental Table S3). The reduction of these mRNAs and proteins was confirmed by real-time PCR and immunoblot analysis (Figure 4, A and B). Survivin is a component of the chromosomal passenger complex (CPC). The CPC regulates diverse mitotic processes and is composed of aurora kinase B and three noncatalytic subunits: survivin, INCENP, and borealin/CDCA8 (Vader *et al.*, 2006; Ruchaud *et al.*, 2007). Dysfunction of the CPC results in chromosome arm resolution defects and failure of cytokinesis (Carvalho *et al.*, 2003; Lens *et al.*, 2003; Gimenez-Abian *et al.*, 2004; McGuinness *et al.*, 2005). Indeed, treatment with ZM447439, an aurora kinase B inhibitor, caused arm resolution defects and failure of cytokinesis (Figure 4, F and G, and data not shown). PRC1 regulates cytokinesis and its knockdown leads to failure of cytokinesis (Mollinari *et al.*, 2005). These results show that UAP56*i* and URH49*i* lead to the down-regulation of genes necessary for mitotic progression, which is consistent with the mitotic defects observed in UAP56*i* and URH49*i* cells.

UAP56 Is Preferentially Associated with the hTHO Complex and Aly, Whereas URH49 Is Preferentially Associated with CIP29

To investigate the differences between UAP56 and URH49, their cellular localization was examined. Endogenous (Figure 5A) and FLAG-tagged UAP56 and URH49 (Supplemental Figure S4A) localized to the nucleus, as previously described (Kota *et al.*, 2008). EGFP-UAP56 and DsRed-URH49
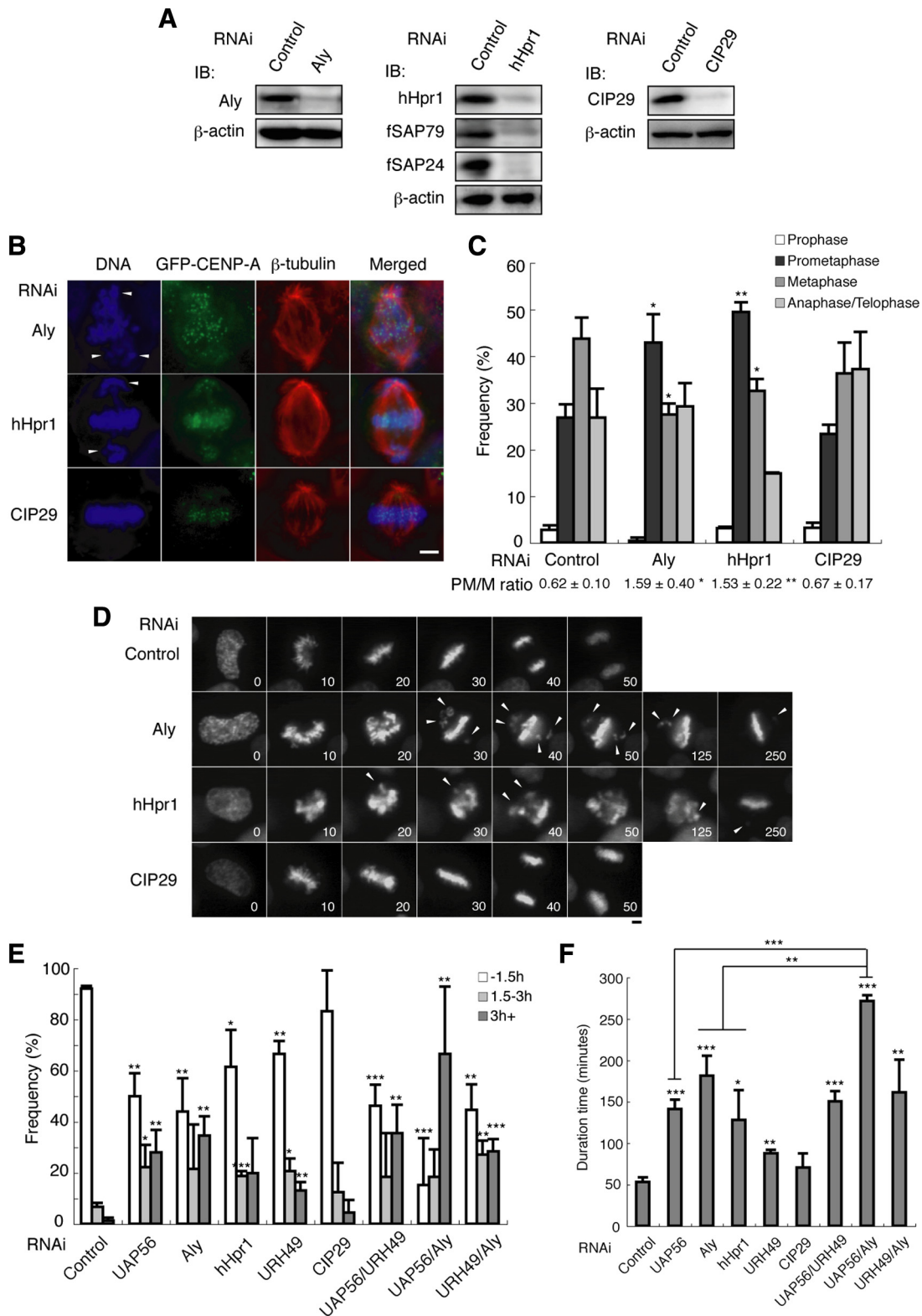
Figure 6. hTREX*i* results in mitotic delay with chromosome misalignment. (A) Knockdown of Aly, hHpr1 or CIP29 was confirmed by immunoblotting. HeLa cells transfected with the indicated siRNAs were cultured for 48 h. β-actin was used as a loading control. IB; immunoblotting. (B) Typical mitotic figures are shown in the indicated siRNA-transfected HeLa cells expressing GFP-CENP-A. GFP-CENP-A and β-tubulin signals indicate the location of the centromere and spindle body, respectively. The arrowhead indicates the misaligned chromosome. Scale bar, 10 μm. (C) The proportion of cells in each mitotic phase is shown in several knockdown cells. Each value is the mean with SD of three independent experiments (more than 70 cells were evaluated in each experiment). The ratios of cells in prometaphase to metaphase (PM/M ratio) are shown as the means with SD of three independent experiments. p values were calculated by comparison with the control: *p < 0.05, **p < 0.01, Student's *t* test. (D) Representative successive live cell images in knockdown cells. The number at the

also colocalized to the nucleus (Figure 5A). These data indicate that UAP56 and URH49 localized in the same, nuclear compartment.

To compare the factors associated with UAP56 and URH49, immunoprecipitation was performed using anti-UAP56– or anti-URH49–specific antibodies. Endogenous UAP56 coimmunoprecipitated the hTHO components fSAP79 and Aly, but not URH49 and CIP29 (Figure 5B). On the other hand, endogenous URH49 coimmunoprecipitated CIP29, but not fSAP79, UAP56, and Aly. It has been shown that the hTREX complex binds to the CBC via an interaction between Aly and the CBC (Cheng *et al.,* 2006). We detected an association between UAP56 and CBP80, a component of the CBC, but failed to detect an interaction between URH49 and CBP80 (Figure 5B). To confirm further, we performed several biochemical purification and immunoblot experiments using FLAG-UAP56 and FLAG-URH49 stable clones, tandem affinity purification using FLAG-UAP56-TAP and FLAG-URH49-TAP, and His-UAP56 and His-URH49 pulldown experiments (Supplemental Figure S4, B–D). All the results clearly showed that UAP56 associated with the hTHO components and Aly rather than CIP29, whereas URH49 preferentially associated with CIP29. We note that URH49 weakly interacted with Aly and that UAP56 also slightly interacted with CIP29, but that these interactions were weak compared with those with UAP56 and URH49, respectively (Supplemental Figure S4, B and D).

Immunoprecipitation with antibodies against endogenous hTho2, fSAP79, Aly, and CIP29 indicated that hTho2 and fSAP79 copurified with UAP56 and Aly, and Aly also copurified with the hTHO components and UAP56, as previously reported (Figure 5C; Masuda *et al.,* 2005; Cheng *et al.,* 2006). The hTHO components and Aly copurified with URH49 very slightly, but not with CIP29 (Figure 5C). In contrast, CIP29 copurified with URH49, but interactions between CIP29 and the hTHO complex, as well as between CIP29 and Aly, were not observed. Taken together, UAP56 preferentially binds the hTHO complex and Aly to form the TREX complex, whereas URH49 preferentially binds CIP29, therefore forming a novel URH49–CIP29 complex. We named the URH49–CIP29 complex the AREX complex (Figure 5D).

hTHOi and Alyi Cause Mitotic Delay with Chromosome Misalignment and PMSCS, Whereas CIP29i Causes Chromosome Arm Resolution Defects

To reveal the in vivo biological functions of the hTREX complex and the AREX complex, the hTHO complex, Aly, and CIP29 were knocked down in HeLa cells. Each siRNA efficiently knocked down its corresponding mRNA and protein (Figure 6A). In hHpr1i cells, the expression of fSAP79

and fSAP24, other components of the hTREX complex, was down-regulated. A similar phenomenon was previously observed in *S. cerevisiae* lacking the THO components (Strasser *et al.,* 2002). Immunodepletion of hTho2 from HeLa cell NE also codepleted the rest of the THO components (Masuda *et al.,* 2005). Together, this implies that the THO complex is unstable if one of its components is depleted. In these cells, the effect on nuclear export of bulk poly(A)$^+$ RNA was examined. hHpr1i, Alyi, and CIP29i cells accumulated bulk poly(A)$^+$ RNA in the nucleus (Supplemental Figure S5). This suggests that CIP29 is involved in the mRNA export pathway.

The effects on mitotic progression in knockdown cells were examined by the observation of cells expressing GFP-CENP-A (Figure 6, B and C) and live cell imaging of an H2B-GFP–expressing cell line (Figure 6, D–F and Supplemental Movies S4–S6). These data indicated that Alyi and hHpr1i caused mitotic delay with chromosome misalignment. On the other hand, CIP29i did not cause significant mitotic delay. In addition, upon knockdown of hHpr1 and Aly, sister chromatids were often prematurely separated (Figure 7, B and C). In addition, PMSCS occurred after treatment with siRNAs targeting different sites on *Aly* and after siRNA treatment against *hTho2*, a component of the hTHO complex (Supplemental Figure S3, C and D). These results indicate that PMSCS is the cause of chromosome misalignment in hTREXi cells. In contrast, CIP29i cells rarely exhibited PMSCS, but sister chromatids were often attached at the chromosome arms in CIP29i cells (Figure 7, B and D, and Supplemental Figure S3, C and E). These results clearly showed that Alyi and hTHOi led to mitotic defects similar to those observed in UAP56i cells and that CIP29i led to defects similar to those observed in URH49i cells.

Combined hTREXi and AREXi Does Not Lead to Additional Mitotic Defects Compared with Single Knockdown, Whereas Double Knockdown of Components of the Same Complex Leads to Severe Mitotic Defects

If the function of the AREX complex is redundant with that of the hTREX complex, the mitotic defects in hTREXi cells might be enhanced by codepletion of an AREX component. From live cell imaging analysis, the combination of UAP56i and URH49i did not cause additional mitotic delay compared with that in UAP56i-only cells (Figure 6, E and F). In addition, the combination of Alyi and URH49i gave a similar result to Alyi-only cells. Next, double knockdown of hTREX components and AREX components was examined by mitotic chromosome spread analysis. Knockdown combinations of an hTREX component and an AREX component resulted in PMSCS. These results indicate that the phenotype of hTREXi dominates that of AREXi. The frequency and severity of PMSCS in these knockdowns were similar to those in the corresponding single hTREXi cells (Figure 7C), suggesting that there was no effect of additional knockdown of the AREX complex. These data suggest that the hTREX complex has a unique role related to PMSCS, which is distinct from the role of the AREX complex.

In contrast, double knockdown of UAP56 and Aly led to frequent, prolonged mitotic arrest during prometaphase compared with either single knockdown (Figure 6, E and F). In addition, double knockdown of the hTREX components (denoted "hTREXi combination") led to more severe PMSCS than the corresponding single hTREXi (Figure 7, B and C). Similarly, double knockdown of the AREX components resulted in defects of chromosome arm resolution and failure of cytokinesis more frequently than did either single knockdown (Figure 7D and Supplemental Figure S2B). These re-

Figure 6 (cont). bottom right indicates the time (min) from nuclear envelope breakdown (NEBD). The arrowhead indicates the misaligned chromosome. Scale bar, 10 μm. (E) The time from NEBD-to-anaphase transition or mitotic cell death (MCD) was measured. At least 30 cells were observed in each experiment. Each value is the mean with SD of three independent experiments. The data from Figure 2D for Control and UAP56, and URH49 knockdown cells are shown to enable comparison. p values were calculated by comparison with the control: *p < 0.05, **p < 0.01, ***p < 0.001, Student's *t* test. (F) The duration is shown as the mean with SD of three independent experiments. The data from Figure 2E for Control and UAP56 and URH49 knockdown cells are shown to enable comparison. p values were calculated by comparison with the control if not indicated otherwise: *p < 0.05, **p < 0.01, ***p < 0.001, Student's *t* test.
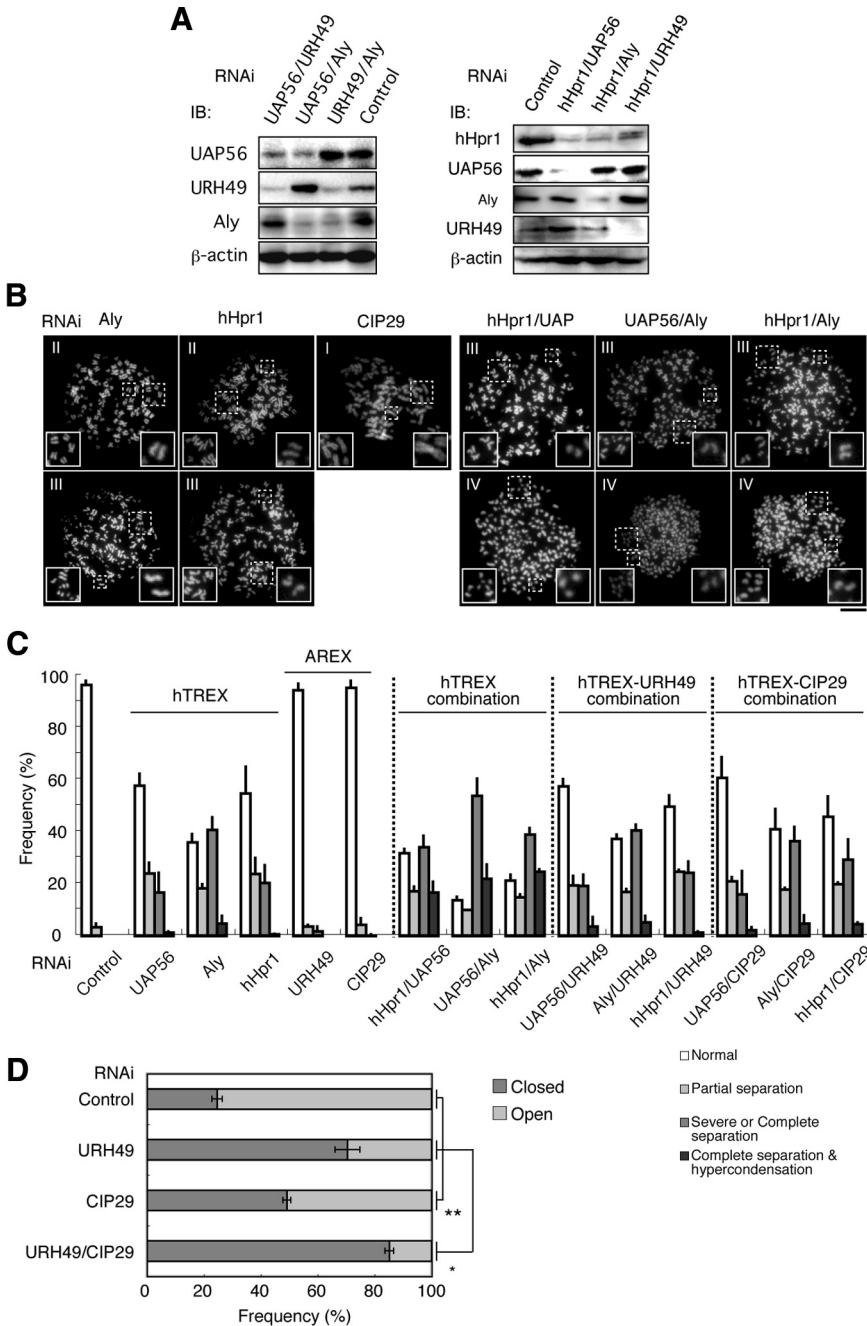
Figure 7. hTREX*i* leads to PMSCS, while AREX*i* leads to chromosome arm resolution defects. (A) Combined knockdowns were confirmed by immunoblotting. β-actin was used as a loading control. IB, immunoblotting. (B) Representative mitotic chromosome spreads in knockdown cells. The Roman numeral in the top left represents the category as defined in Figure 3A. The bottom left and right insets represent medium- and high-magnification images of the mitotic chromosome spread(s) indicated by the large and small dashed squares, respectively. Scale bar, 10 μm. (C) The frequency of PMSCS was classified I to IV after analyzing more than 100 cells. Each value is the mean with SD of three independent experiments. The data from Figure 3C for Control and UAP56 and URH49 knockdown cells are shown to enable comparison. (D) The frequency of mitotic chromosomes with open and closed arms was obtained by analyzing more than 100 cells in each experiment. Each value is the mean with SD of three independent experiments. The data from Figure 3E for Control and URH49 knockdown cells are shown to enable comparison. p values: *p < 0.05, **p < 0.01, Student's *t* test.

sults suggest that double knockdown inhibited the function of the hTREX complex or the AREX complex more effectively than did single knockdown. Thus, the hTREX complex is required for mitotic progression and sister chromatid cohesion, whereas the AREX complex is required for chromosome arm resolution and cytokinesis.

DISCUSSION

Either UAP56 or URH49 can rescue the lethality of the Sub2 deletion strain in *S. cerevisiae*, and both are required for bulk poly(A)$^+$ RNA export, implying that UAP56 and URH49 have a similar function. Therefore, it has been unclear whether UAP56 and URH49 have different biochemical

characteristics and physiological roles. Here, we showed that specific knockdown of UAP56 and URH49 affected the expression of different sets of genes and caused different mitotic defects despite their extensive sequence homology. In addition, UAP56 and URH49 mostly form different complexes: the TREX complex and the AREX complex, respectively. These complexes individually regulate different steps of mitotic progression. These data clearly indicate that UAP56 and URH49 have unique functions in vivo as well as a redundant function.

Our data suggest that the mRNA export machineries are linked to mitotic processes. The reduction in mitotic factors, such as claspin and BRCA1 in UAP56*i* cells, and survivin and PRC1 in URH49*i* cells, could explain the phenotype of

mitotic defects associated with dysfunction of UAP56 or URH49. The microarray data showed that UAP56*i* and URH49*i* also resulted in reductions in other mitotic factors, which might contribute to the mitotic defects. These results provide evidence to support the model that UAP56 and URH49 regulate mitotic progression by forming a specific mRNA processing/export pathway for the expression of key regulators of mitosis.

We also examined several other possibilities that could cause mitotic defects in hTREX*i* and AREX*i* cells. The nuclear accumulation of bulk poly(A)$^+$ RNA per se, which was induced by several combined knockdowns (Supplemental Figure S5), was not correlated with the degree or type of mitotic defect. Thus, it is unlikely that the mitotic defects were a secondary consequence of a defect in bulk poly(A)$^+$ RNA export. In addition, we examined another possibility, the direct regulation of mitosis by the hTREX complex and the AREX complex, but we did not obtain evidence for this from the analysis of the localization of the hTREX components and the AREX components during mitosis (Supplemental Results and Supplemental Figures S6 and S7). However, we could not exclude the other possibilities that UAP56 and URH49 directly or indirectly act on mitotic progression. In any case, down-regulation of specific genes required for mitotic progression was correlated with the associated mitotic defects. Thus, we favored the model that reduced expression of particular genes contributes to the mitotic defects in UAP56*i* and URH49*i* cells.

Supporting our model, it has been reported that several mRNA export factors contribute to the regulation of gene expression to facilitate particular biological processes. There is growing evidence that functional subsets of mRNAs are controlled by mRNA export factors (Hieronymus and Silver, 2003; Chakraborty *et al.,* 2008; Wang *et al.,* 2009). In addition, a related hypothesis has proposed the existence of an RNA regulon, in which mRNAs encoding functionally related proteins are posttranscriptionally coregulated by RNA-binding proteins, through binding to a specific sequence on target mRNAs (Keene, 2007). TREX components have been implicated in several mRNA maturation processes, including the coupling of transcription and splicing to export, pre-mRNA splicing and mRNA packaging and turnover (Jensen *et al.,* 2003; Reed and Cheng, 2005; Shen *et al.,* 2008). Future research into target gene regulation by UAP56 and URH49 should provide insight into these processes.

Genome-wide RNAi screening in the *D. melanogaster* S2 cell line has shown that some mRNA export factors affect aspects of mitotic progression, such as chromosome alignment, spindle formation, and cytokinesis. Among them, knockdown of *Hel25E,* the *Drosophila* UAP56 homolog, and *Drosophila Tho2* result in chromosome misalignment (Goshima *et al.,* 2007; Somma *et al.,* 2008). It has also been reported that Hel25E suppressed the phenotype of an *S. pombe* strain, *wee1*/cdc25+ or *wee1/mik1,* which undergoes mitotic catastrophe by premature entry into mitosis (Warbrick and Glover, 1994). In addition to the TREX components, knockdown and mutation of *Sbr,* a Tap homolog, respectively, cause defects in mitotic spindle formation and cytokinesis and defects in meiotic spindle formation and chromosome alignment (Kwon *et al.,* 2008; Golubkova *et al.,* 2009). Most recently, the exon junction complex component Magoh has been shown to control neural stem cell division through regulating the expression of the key mitotic regulator *Lis1* (Silver *et al.,* 2010). Therefore, the functional importance of the mRNA processing/export machinery in mitotic progression is evident and is evolutionarily conserved. Our study

has shed light on the importance of the mRNA processing/export machinery for faithful chromosome segregation.

In *S. cerevisiae,* Sub2 is recruited to transcription sites by the THO complex. When the THO complex is disrupted, Tho1, a homolog of CIP29, functionally substitutes for the THO complex and supports the recruitment of Sub2 onto RNA (Jimeno *et al.,* 2006). Therefore, it is plausible that, in humans, the hTHO complex mainly functions to facilitate the loading of UAP56 onto mRNA, whereas CIP29 facilitates the loading of URH49 onto mRNA, thus forming a different mRNA processing/export pathway. CIP29 was a preferential binding partner for URH49, and both URH49 and CIP29 were required for bulk poly(A)$^+$ RNA export. These findings suggest that the AREX complex has emerged during evolution and forms an mRNA processing/export machinery with a novel function, distinct from that of the hTREX complex.

URH49 and CIP29 are of different importance in the AREX complex, because CIP29*i* did not lead to mitotic progression defects, and the chromosome arm resolution defects were milder in CIP29*i* cells than in URH49*i* cells. These results may imply that there is a hierarchy within the AREX complex. Indeed, URH49 helicase activity is enhanced by CIP29 (Sugiura *et al.,* 2007b). Thus, the function of the AREX complex may largely depend on URH49.

UAP56 is continuously expressed during the cell cycle, whereas URH49 is expressed at lower levels in the quiescent phase, yet becomes increasingly expressed in the cell proliferation phase in cultured mammalian cells. In addition, URH49 is expressed at lower levels than UAP56 in most tissues, but is highly expressed in the testis (Pryor *et al.,* 2004). Recently, in situ hybridization revealed that *Xenopus laevis DDX39* (a URH49 homolog) mRNA is strictly localized to a subpopulation of proliferating cells in developmental and regenerating tissues (Wilson *et al.,* 2010). CIP29, like URH49, is also highly expressed in the testis and is up-regulated in the cell proliferation phase (Choong *et al.,* 2001; Fukuda *et al.,* 2002; Fukuda and Pelus, 2005), implying that the AREX complex may constitute a tissue-specific and cell proliferation-associated mRNA processing/export machinery.

It has been reported that URH49 and CIP29 are overexpressed in several cancers (Choong *et al.,* 2001; Lu *et al.,* 2007; Pujana *et al.,* 2007; Sugiura *et al.,* 2007a; Montero-Conde *et al.,* 2008). Interestingly, the expression levels of survivin and PRC1, which were down-regulated in URH49*i* cells, are strongly associated with several types of cancer and are important for cancer cell survival. Survivin is a molecular target for cancer therapy, and its inhibitors have been developed for use as anticancer drugs (Altieri, 2008). Survivin is also up-regulated in the cell proliferation phase, as are URH49 and CIP29. In addition, PRC1 is up-regulated in breast and bladder cancer cells and is also expressed in normal testis tissue (Kanehira *et al.,* 2007; Shimo *et al.,* 2007). Therefore, it is likely that the AREX complex plays a role in tumor progression through the regulation of *survivin* and *PRC1* mRNA and therefore protein expression. The AREX complex may have a specialized role in cell proliferation–associated biological processes, such as tumor progression.

In humans, several key mRNA export factors have evolutionarily diversified compared with those in yeast. In addition to UAP56 and URH49, several mRNA export factors such as Tap, p15/NXT, Dbp5/DDX19, and SR proteins form gene families in humans (Stutz and Izaurralde, 2003; Barbosa-Morais *et al.,* 2006; Wolyniak and Cole, 2008). To date, the functional redundancy and differences within these families remain largely unknown. We have demonstrated that

the closely related mRNA export factors UAP56 and URH49 preferentially form different nuclear complexes to regulate different sets of mRNAs, and that these complexes are linked to specific cellular processes. It is likely that future studies will reveal that multiple mRNA processing/export pathways function as one of the regulatory steps in achieving posttranscriptional gene regulation in higher organisms.

ACKNOWLEDGMENTS

REFERENCES

Abmayr, S. M., and Workman, J. L. (1993). Preparation of nuclear and cytoplasmic extracts from mammalian cells. Curr. Protoc. Mol. Biol. *2*(Unit 12.1), 1–9.

Aguilera, A. (2005). Cotranscriptional mRNP assembly: from the DNA to the nuclear pore. Curr. Opin. Cell Biol. *17*, 242–250.

Altieri, D. C. (2008). Survivin, cancer networks and pathway-directed drug discovery. Nat. Rev. Cancer *8*, 61–70.

Andrews, N. C., and Faller, D. V. (1991). A rapid micropreparation technique for extraction of DNA-binding proteins from limiting numbers of mammalian cells. Nucleic Acids Res. *19*, 2499.

Barbosa-Morais, N. L., Carmo-Fonseca, M., and Aparicio, S. (2006). Systematic genome-wide annotation of spliceosomal proteins reveals differential gene family expansion. Genome Res. *16*, 66–77.

Carvalho, A., Carmena, M., Sambade, C., Earnshaw, W. C., and Wheatley, S. P. (2003). Survivin is required for stable checkpoint activation in taxol-treated HeLa cells. J. Cell Sci. *116*, 2987–2998.

Chabalier, C., Lamare, C., Racca, C., Privat, M., Valette, A., and Larminat, F. (2006). BRCA1 downregulation leads to premature inactivation of spindle checkpoint and confers paclitaxel resistence. Cell Cycle *5*, 1001–1007.

Chakraborty, P., Wang, Y., Wei, J. H., van Deursen, J., Yu, H., Malureanu, L., Dasso, M., Forbes, D. J., Levy, D. E., Seemann, J., and Fontoura, B. M. (2008). Nucleoporin levels regulate cell cycle progression and phase-specific gene expression. Dev. Cell *15*, 657–667.

Cheng, H., Dufu, K., Lee, C. S., Hsu, J. L., Dias, A., and Reed, R. (2006). Human mRNA export machinery recruited to the 5' end of mRNA. Cell *127*, 1389–1400.

Choong, M. L., Tan, L. K., Lo, S. L., Ren, E. C., Ou, K., Ong, S. E., Liang, R. C., Seow, T. K., and Chung, M. C. (2001). An integrated approach in the discovery and characterization of a novel nuclear protein over-expressed in liver and pancreatic tumors. FEBS Lett. *496*, 109–116.

Cullen, B. R. (2003). Nuclear RNA export. J. Cell Sci. *116*, 587–597.

DeLuca, J. G., Moree, B., Hickey, J. M., Kilmartin, J. V., and Salmon, E. D. (2002). hNuf2 inhibition blocks stable kinetochore-microtubule attachment and induces mitotic cell death in HeLa cells. J. Cell Biol. *159*, 549–555.

Farny, N. G., Hurt, J. A., and Silver, P. A. (2008). Definition of global and transcript-specific mRNA export pathways in metazoans. Genes Dev. *22*, 66–78.

Fukuda, S., and Pelus, L. M. (2005). Growth inhibitory effect of Hcc-1/CIP29 is associated with induction of apoptosis, not just with G2/M arrest. Cell Mol. Life Sci. *62*, 1526–1527.

Fukuda, S., Wu, D. W., Stark, K., and Pelus, L. M. (2002). Cloning and characterization of a proliferation-associated cytokine-inducible protein, CIP29. Biochem. Biophys. Res. Commun. *292*, 593–600.

Gilman, M. (1997). Preparation of cytoplasmic RNA from tissue culture cells. Curr. Protoc. Mol. Biol. *1*(Unit 4.1), 1–6.

Gimenez-Abian, J. F., Sumara, I., Hirota, T., Hauf, S., Gerlich, D., de la Torre, C., Ellenberg, J., and Peters, J. M. (2004). Regulation of sister chromatid cohesion between chromosome arms. Curr. Biol. *14*, 1187–1193.

Golubkova, E. V., Markova, E. G., Markov, A. V., Avanesyan, E. O., Nokkala, S., and Mamon, L. A. (2009). Dm *nxf1/sbr* gene affects the formation of meiotic spindle in female *Drosophila melanogaster.* Chromosome Res. *17*, 833–845.

Goshima, G., Wollman, R., Goodwin, S. S., Zhang, N., Scholey, J. M., Vale, R. D., and Stuurman, N. (2007). Genes required for mitotic spindle assembly in *Drosophila* S2 cells. Science *316*, 417–421.

Hautbergue, G. M., Hung, M. L., Walsh, M. J., Snijders, A. P., Chang, C. T., Jones, R., Ponting, C. P., Dickman, M. J., and Wilson, S. A. (2009). UIF, a New mRNA export adaptor that works together with REF/ALY, requires FACT for recruitment to mRNA. Curr. Biol. *19*, 1918–1924.

Herold, A., Teixeira, L., and Izaurralde, E. (2003). Genome-wide analysis of nuclear mRNA export pathways in *Drosophila.* EMBO J. *22*, 2472–2483.

Hieronymus, H., and Silver, P. A. (2003). Genome-wide analysis of RNA-protein interactions illustrates specificity of the mRNA export machinery. Nat. Genet. *33*, 155–161.

Holland, A. J., and Cleveland, D. W. (2009). Boveri revisited: chromosomal instability, aneuploidy and tumorigenesis. Nat. Rev. Mol. Cell Biol. *10*, 478–487.

Huang, Y., Gattoni, R., Stevenin, J., and Steitz, J. A. (2003). SR splicing factors serve as adapter proteins for TAP-dependent mRNA export. Mol. Cell *11*, 837–843.

Jensen, T. H., Dower, K., Libri, D., and Rosbash, M. (2003). Early formation of mRNP: license for export or quality control. Mol. Cell *11*, 1129–1138.

Jimeno, S., Luna, R., Garcia-Rubio, M., and Aguilera, A. (2006). Tho1, a novel hnRNP, and Sub2 provide alternative pathways for mRNP biogenesis in yeast THO mutants. Mol. Cell. Biol. *26*, 4387–4398.

Jimeno, S., Rondon, A. G., Luna, R., and Aguilera, A. (2002). The yeast THO complex and mRNA export factors link RNA metabolism with transcription and genome instability. EMBO J. *21*, 3526–3535.

Kanehira, M., Katagiri, T., Shimo, A., Takata, R., Shuin, T., Miki, T., Fujioka, T., and Nakamura, Y. (2007). Oncogenic role of MPHOSPH1, a cancer-testis antigen specific to human bladder cancer. Cancer Res. *67*, 3276–3285.

Kapadia, F., Pryor, A., Chang, T. H., and Johnson, L. F. (2006). Nuclear localization of poly(A)+ mRNA following siRNA reduction of expression of the mammalian RNA helicases UAP56 and URH49. Gene *15*, 37–44.

Katahira, J., Inoue, H., Hurt, E., and Yoneda, Y. (2009). Adaptor Aly and co-adaptor Thoc5 function in the Tap-p15-mediated nuclear export of HSP70 mRNA. EMBO J. *28*, 556–567.

Katahira, J., Strasser, K., Podtelejnikov, A., Mann, M., Jung, J. U., and Hurt, E. (1999). The Mex67p-mediated nuclear mRNA export pathway is conserved from yeast to human. EMBO J. *18*, 2593–2609.

Keene, J. D. (2007). RNA regulons: coordination of post-transcriptional events. Nat. Rev. Genet. *8*, 533–543.

Kohler, A., and Hurt, E. (2007). Exporting RNA from the nucleus to the cytoplasm. Nat. Rev. Mol. Cell Biol. *8*, 761–773.

Komili, S., and Silver, P. A. (2008). Coupling and coordination in gene expression processes: a systems biology view. Nat. Rev. Genet. *9*, 38–48.

Kota, K. P., Wagner, S. R., Huerta, E., Underwood, J. M., and Nickerson, J. A. (2008). Binding of ATP to UAP56 is necessary for mRNA export. J. Cell Sci. *121*, 1526–1537.

Kwon, M., Godinho, S. A., Chandhok, N. S., Ganem, N. J., Azioune, A., Thery, M., and Pellman, D. (2008). Mechanisms to suppress multipolar divisions in cancer cells with extra centrosomes. Genes Dev. *22*, 2189–2203.

Leaw, C. L., Ren, E. C., and Choong, M. L. (2004). Hcc-1 is a novel component of the nuclear matrix with growth inhibitory function. Cell. Mol. Life Sci. *61*, 2264–2273.

Lens, S. M., Wolthuis, R. M., Klompmaker, R., Kauw, J., Agami, R., Brummelkamp, T., Kops, G., and Medema, R. H. (2003). Survivin is required for a sustained spindle checkpoint arrest in response to lack of tension. EMBO J. *22*, 2934–2947.

Lu, Y., Yi, Y., Liu, P., Wen, W., James, M., Wang, D., and You, M. (2007). Common human cancer genes discovered by integrated gene-expression analysis. PLoS One *2*, e1149.

Luo, M. L., Zhou, Z., Magni, K., Christoforides, C., Rappsilber, J., Mann, M., and Reed, R. (2001). Pre-mRNA splicing and mRNA export linked by direct interactions between UAP56 and Aly. Nature *413*, 644–647.

MacMorris, M., Brocker, C., and Blumenthal, T. (2003). UAP56 levels affect viability and mRNA export in *Caenorhabditis elegans.* RNA *9*, 847–857.

Maniatis, T., and Reed, R. (2002). An extensive network of coupling among gene expression machines. Nature *416*, 499–506.

Masuda, S., Das, R., Cheng, H., Hurt, E., Dorman, N., and Reed, R. (2005). Recruitment of the human TREX complex to mRNA during splicing. Genes Dev. 19, 1512–1517.

McGuinness, B. E., Hirota, T., Kudo, N. R., Peters, J. M., and Nasmyth, K. (2005). Shugoshin prevents dissociation of cohesin from centromeres during mitosis in vertebrate cells. PLoS Biol 3, e86.

Mollinari, C., Kleman, J. P., Saoudi, Y., Jablonski, S. A., Perard, J., Yen, T. J., Margolis, R. L. (2005). Ablation of PRC1 by small interfering RNA demonstrates that cytokinetic abscission requires a central spindle bundle in mammalian cells, whereas completion of furrowing does not. Mol. Biol. Cell 16, 1043–1055.

Montero-Conde, C., et al. (2008). Molecular profiling related to poor prognosis in thyroid carcinoma. Combining gene expression data and biological information. Oncogene 27, 1554–1561.

Musacchio, A., and Salmon, E. D. (2007). The spindle-assembly checkpoint in space and time. Nat. Rev. Mol. Cell Biol. 8, 379–393.

Nojima, T., Hirose, T., Kimura, H., and Hagiwara, M. (2007). The interaction between cap-binding complex and RNA export factor is required for intronless mRNA export. J. Biol. Chem. 282, 15645–15651.

Onn, I., Heidinger-Pauli, J. M., Guacci, V., Unal, E., and Koshland, D. E. (2008). Sister chromatid cohesion: a simple concept with a complex reality. Annu. Rev. Cell Dev. Biol. 24, 105–129.

Orphanides, G., and Reinberg, D. (2002). A unified theory of gene expression. Cell 108, 439–451.

Peters, J. M., Tedeschi, A., and Schmitz, J. (2008). The cohesin complex and its roles in chromosome biology. Genes Dev. 22, 3089–3114.

Pryor, A., Tung, L., Yang, Z., Kapadia, F., Chang, T. H., and Johnson, L. F. (2004). Growth-regulated expression and G0-specific turnover of the mRNA that encodes URH49, a mammalian DExH/D box protein that is highly related to the mRNA export protein UAP56. Nucleic Acids Res. 32, 1857–1865.

Pujana, M. A., et al. (2007). Network modeling links breast cancer susceptibility and centrosome dysfunction. Nat. Genet. 39, 1338–1349.

Reed, R., and Cheng, H. (2005). TREX, SR proteins and export of mRNA. Curr. Opin. Cell Biol. 17, 269–273.

Reed, R., and Hurt, E. (2002). A conserved mRNA export machinery coupled to pre-mRNA splicing. Cell 108, 523–531.

Rodrigues, J. P., Rode, M., Gatfield, D., Blencowe, B. J., Carmo-Fonseca, M., and Izaurralde, E. (2001). REF proteins mediate the export of spliced and unspliced mRNAs from the nucleus. Proc. Natl. Acad. Sci. USA 98, 1030–1035.

Ruchaud, S., Carmena, M., and Earnshaw, W. C. (2007). Chromosomal passengers: conducting cell division. Nat. Rev. Mol. Cell Biol. 8, 798–812.

Shen, H., Zheng, X., Shen, J., Zhang, L., Zhao, R., and Green, M. R. (2008). Distinct activities of the DExD/H-box splicing factor hUAP56 facilitate stepwise assembly of the spliceosome. Genes Dev. 22, 1796–1803.

Shimo, A., Nishidate, T., Ohta, T., Fukuda, M., Nakamura, Y., and Katagiri, T. (2007). Elevated expression of protein regulator of cytokinesis 1, involved in the growth of breast cancer cells. Cancer Sci. 98, 174–181.

Silver, D. L., et al. (2010). The exon junction complex component Magoh controls brain size by regulating neural stem cell division. Nat. Neurosci. 13, 551–558.

Skibbens, R. V. (2008). Cell biology of cancer: BRCA1 and sister chromatid pairing reactions? Cell Cycle 15, 449–452.

Somma, M. P., et al. (2008). Identification of Drosophila mitotic genes by combining co-expression analysis and RNA interference. PLoS Genet 4, e1000126.

Strasser, K., and Hurt, E. (2001). Splicing factor Sub2p is required for nuclear mRNA export through its interaction with Yra1p. Nature 413, 648–652.

Strasser, K., et al. (2002). TREX is a conserved complex coupling transcription with messenger RNA export. Nature 417, 304–308.

Stutz, F., and Izaurralde, E. (2003). The interplay of nuclear mRNP assembly, mRNA surveillance and export. Trends Cell Biol. 13, 319–327.

Sugiura, T., Nagano, Y., and Noguchi, Y. (2007a). DDX39, upregulated in lung squamous cell cancer, displays RNA helicase activities and promotes cancer cell growth. Cancer Biol. Ther. 6, 957–964.

Sugiura, T., Sakurai, K., and Nagano, Y. (2007b). Intracellular characterization of DDX39, a novel growth-associated RNA helicase. Exp. Cell Res. 313, 782–790.

Tang, Z., Shu, H., Qi, W., Mahmood, N. A., Mumby, M. C., and Yu, H. (2006). PP2A is required for centromeric localization of Sgo1 and proper chromosome segregation. Dev. Cell 10, 575–585.

Vader, G., Medema, R. H., and Lens, S. M. (2006). The chromosomal passenger complex: guiding Aurora-B through mitosis. J. Cell Biol. 173, 833–837.

Valencia, P., Dias, A. P., and Reed, R. (2008). Splicing promotes rapid and efficient mRNA export in mammalian cells. Proc. Natl. Acad. Sci. USA 105, 3386–3391.

Vinciguerra, P., and Stutz, F. (2004). mRNA export: an assembly line from genes to nuclear pores. Curr. Opin. Cell Biol. 16, 285–292.

Wang, X., Chinnam, M., Wang, J., Wang, Y., Zhang, X., Marcon, E., Moens, P., and Goodrich, D. W. (2009). Thoc1 deficiency compromises gene expression necessary for normal testis development in the mouse. Mol. Cell. Biol. 29, 2794–2803.

Warbrick, E., and Glover, D. (1994). A Drosophila gene encoding a DEAD box RNA helicase can suppress loss of wee1/mik1 function in Schizosaccharomyces pombe. Mol. Gen. Genet. 245, 654–657.

Warren, C. D., Eckley, D. M., Lee, M. S., Hanna, J. S., Hughes, A., Peyser, B., Jie, C., Irizarry, R., and Spencer, F. A. (2004). S-phase checkpoint genes safeguard high-fidelity sister chromatid cohesion. Mol. Biol. Cell 15, 1724–1735.

Wilson, J. M., Martinez-De Luna, R. I., El Hodiri, H. M., Smith, R., King, M. W., Mescher, A. L., Neff, A. W., and Belecky-Adams, T. L. (2010). RNA helicase Ddx39 is expressed in the developing central nervous system, limb, otic vesicle, branchial arches and facial mesenchyme of Xenopus laevis. Gene Expr. Patterns 10, 44–52.

Wolyniak, M. J., and Cole, C. N. (2008). Harnessing genomics to explore the processes and evolution of mRNA export. RNA Biol. 5, 68–72.

Xu, H., Boone, C., and Klein, H. L. (2004). Mrc1 is required for sister chromatid cohesion to aid in recombination repair of spontaneous damage. Mol. Cell. Biol. 24, 7082–7090.

Yang, Z., Guo, J., Chen, Q., Ding, C., Du, J., and Zhu, X. (2005). Silencing mitosin induces misaligned chromosomes, premature chromosome decondensation before anaphase onset, and mitotic cell death. Mol. Cell. Biol. 25, 4062–4074.